High-resolution interactive global flood forecast for past, present, and future

B. van den Bout [1], F.J. Kolaparambil [1], K. van Roon[2], D. Meijvogel[2]

[1] Twente University, Faculty of Geo-information Science and Earth Observation (ITC), Drienerlolaan 5, 7522 NB Enschede, The Netherlands

2 Fast Hazard, de Linie 588, Apeldoorn, The Netherlands

Corresponding author: B. van den Bout (b.vandenbout@utwente.nl)

Abstract

Globally operating modelling approaches for flood dynamics have shown significant increases in usage, quality and availability in recent years. Flood modelling at global scale stretches the computational demand, due to combinations of spatial scale and resolution, limiting to static pre-computed maps and prohibiting interactivity. Particular high-resolution global models are only available as static information layers, whereas dynamic models operate at lower resolution to address operational shortcomings. In this article, a novel system is described that links a state-of-the-art efficient flood modelling core with an automated global parameterization scheme based on global, bias-corrected and space-based datasets. This combined approach delivers a first-generation, zero configuration flood modelling system capable of producing high-resolution, interactive flood maps. It supports a highly efficient global early warning system for both flash and fluvial floods and enables the generation of historic flood map time series for any location worldwide. The utilized event-based simulation approach has some limitations in applicability to continuous modelling, the system shows major speed increases at near-identical accuracy with global availability.

Keywords: flood, climate, hazard, risk

Highlights

- Real-time global flood map forecasts for flash and fluvial floods at high resolution.
- Global out-of-the-box interactive flood hazard maps.
- An additional 10x speed improvement for larger areas over the previous FastFlood model.

Introduction

Flood modelling can be a time-consuming exercise, requiring vast computational resources and significant expertise on the various interplays between data quality, detail, and the numerical solutions deployed within a particular model. High-applicability flood modelling approaches have emerged in the past decade to provide enriched information layers for various types of applications (e.g. trend analysis, historic baselines, climate analysis, efficient large-scale hazard and risk mapping, portfolio risk management).

Despite the availability of powerful flood-hazard mapping products like JBA's high-resolution flood maps(Bradbrook, 2006), CAMAFlood (Yamazaki et al., 2018) , Fathom (Bates et al., 2018), the Copernicus-based Global Surface Water Explorer (Pekel et al., 2016) , DFO Flood Observatory (Kettner et al., 2021), GLOFAS (Harrigan et al., 2020), and Google's Global Flood Mode (Nearing et al., 2025), these systems typically generate static flood hazard layers or daily-subdaily inundation maps for predefined scenarios. These outputs, while widely used across applications such as trend analysis, historical baselines, climate assessments, large-scale risk mapping, and portfolio risk management, are not designed as interactive or adjustable simulation platforms. Due to the complexity of their modeling pipelines and the substantial computation required, live parameter tuning or scenario editing in real time is generally not feasible. As a result, these systems excel at producing ready-to-use hazard maps but rarely support on-the-fly adjustment of inputs or real-time exploration by non-expert users (Alfieri et al., 2013; Cohen et al., 2024; Google Research, 2024).

~~These models are used widely, as a means of creating flood maps, but predominantly through their primary output products; flood hazard maps or daily maps. These are static layers generated once for various scenarios, or at a daily or sub-daily timestep, and have been used in wide ranges of application. However, due to their complicated systems and sometimes large computational requirements, they do not provide a practically adjustable or interactive simulation tool.~~

The steady improvements in the past decades in this field have been largely supported by a consistent effort to enrich Earth Observation datasets (space-based) and other global datasets to produce consistent global data layers of physically-based variables. These layers are useful for the parameterization of physically-based models. Key datasets include elevation data, which gained a massive boost with the release of Copernicus30, and the various refinements on this (Ho et al., 2025), as well as numerous national high-quality datasets. Similarly, land cover, soil, and water levels are now mapped from space more frequently and in more detail than ever before (e.g. SoilGRIDS v2, Poggio et al., 2021; and WorldCover 10m, Venter et al., 2022), allowing for higher quality modelling setups anywhere in the world.

Besides these improvements, a global parameterization scheme remains lacking. Using these global and EO datasets often remains a labor-intensive undertaking requiring particular expertise on the interplay between the model and the data quality and limitations. Few models (e.g. LisFlood, SFINCS, LISEM) incorporate these datasets as automatically available options, and all require code setups, installation and some configuration. The common need to provide local higher-quality datasets could play a big role here, although some tools provide the global data as a supplementary or default layer, with an option to use custom datasets through a common format.

Additionally, some of the parameterization required for a versatile flood modelling system requires datasets not yet produced; in particular, event-based simulation often makes use of design storms or IDF curves. While these inputs can be a tool for localized analysis of precipitation-driven floods, their application to larger areas encounters fundamental issues with the assumptions underlying the design storm analysis (e.g. homogeneous applicability of point statistics to larger areas). Area reduction factors can be used to scale design events, but no globally covering, consistent dataset exists, and implications in their usage for hydrological modelling are far-reaching. Even lowered homogeneous intensities cannot be used in physically-based infiltration models due to their nonlinearity. Localized variability within events dominates real-world infiltration signals. Another solution, like IDF-curve Extensions, has been suggested based on Intensity-Frequency-Duration-Space-curves (IDFS curves), but a global analysis for such statistics is required to effectively apply and use them on a wider scale (Nabukulu et al., 2025).

Finally, existing systems nearly completely lack true interactivity, meaning that user-provided changes through simple input, preferably made without requiring GIS manipulation of data or particular expertise with other

software, are not possible. Some systems support these types of changes to scenarios by the user, but the flood modelling methods underlying it are not fast enough to support true interactivity on larger scales, even with vast compute resources.

True low-code and no-code solutions would allow for a completely new type of application of flood models, and bring the capacity to implement and test adaptation and mitigation, at the building level or otherwise, to serve completely new sectors.

Problem Statement

Flood modelling systems that provide high-applicability flood maps have advanced in recent decades, but a system with rapid, interactive (one that rapidly provides new output based on selected alternative scenarios), zero configuration autonmated global parameterization (without requiring extensive setup and modelling expertise), global coverage (with pre-processed data for model setup and scenarios) and high resolution (at global scale using 20, 10 or smaller grid cell sizes) does not exist. Several key components are currently missing to facilitate such a system, among which are

- Global model parameterization supporting past, present, and future scenarios
- Automated boundary condition placements and model setup
- Space-appropriate design precipitation and snowmelt scenarios
- Rapid flood model core that allows for interactive changes by users

Objective

In this paper, we introduce and describe the workings of the FastFlood Global system, a novel zero-configuration, global, high-resolution flood model for past, present, and future forecasts. Next, we give a short description of the flood model at the core of the system, which can utilize either the FastFlood rapid time-implicit model or a more traditional saint-venant solver. Additionally, an overview is provided of the various types of events that can be simulated, and how these are then parameterized for historic, present and future periods. The last section describes several case studies of the system, for both past, present and future application of the model, as well as comparative analysis with observations and other modelling systems.

The focus of this article is expressly not on the technical details underlying the various data preprocessing and simulation steps, as other works will be cited to expand in more detail on those (see also Bout et al., 2024). Here we are presenting the general system as something that we believe to be a crucial development direction that will allow a new type of usage for flood models.

Methods

FastFlood Global System Schematic

A schematic overview of the FastFlood global system is provided in Figure 1. This system, itself contained within a single executable code, hosted as an API to provide geotiff output to user requests. The data parameterization and boundary conditions are provided, by default, based on a collection of numerous pre-processed global datasets. Then, the FastFlood model can be used to simulate the actual flow processes, which will return the final output layers.

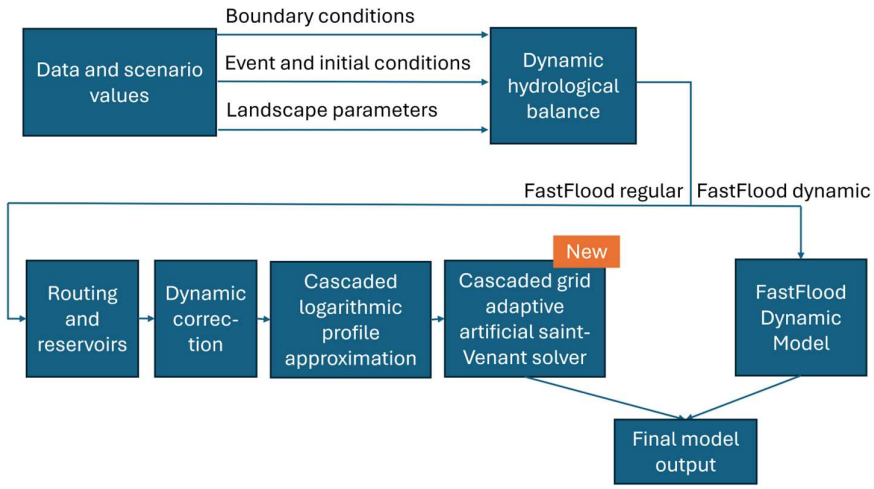

Figure 1 FastFlood Global system schematic view.

FastFlood Model

The core of the system is the time-implicit FastFlood model, a recent innovation in flood modelling approaches. At its core, it by-passes explicit time-stepping in regular solutions to flood dynamics by solving immediately for peak-of-intensity during the event. This leverages an adapted physically-based solver that allows for super-fast simulation of flood hazard maps. It achieves a speed increase of over 20 thousand times on average compared to a traditional flood model (see Appendix A, including the changes presented in this methods section). This speed increase derives predominantly from the manner in which the model directly computes the peak flood depths, peak velocities, and durations. As a trade-off in not carrying out explicit time-stepping, some limitations are present in the case of temporal dynamics that deviate from real solutions, in particular for events with dominant wave dynamics.

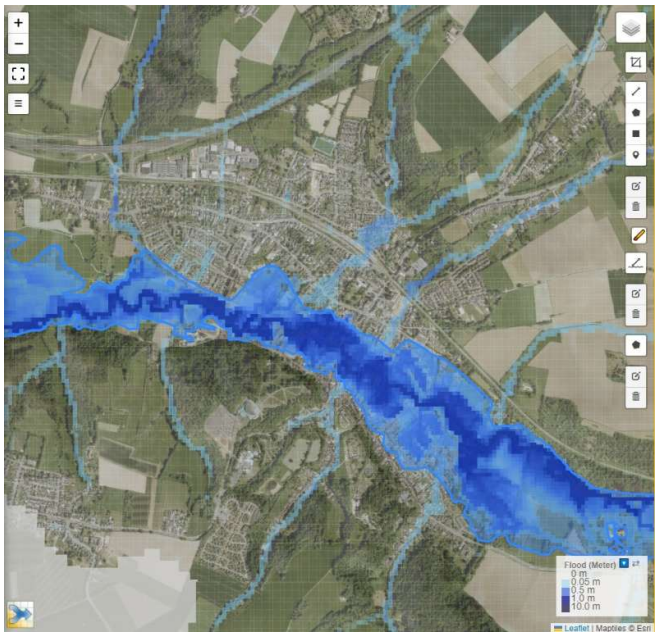

Figure 2 FastFlood.org model applied to the floods in the Geul river, South-Netherlands, 2021

Several aspects of the model have been adjusted, with a focus on combined accuracy and efficiency. Each of these will be further detailed in the sections below.

- Process-dependent grid adjustment
- A cascaded grid for the final artificial Saint-Venant solver

Cascaded-grid adaptive artificial Saint-Venant solver

The first adaptation to the FastFlood model is the usage of process-dependent grids. Input layers, while provided at high resolutions to make parameterization uniform and consistent, are reprocessed to lower resolutions on-the-fly. These lower-resolution grids are then used to solve processes that do not require the full resolution demanded by the final flow dynamics solver. Currently, hydrological and zone-based processes (soil zones, for example) are calculated at the lowest resolution, a factor 9 lower, and river routing and reservoir calculations are carried out at

a factor 3 lower resolution. The factors 3 and 9 are used here as a consequence of the factor-3 scaling and interpolation that is used. For most required variables, averaging is carried out as an interpolation operation, but particular variables involved in non-linear processes can not be averaged, as it would alter the effective outcomes of the model[1]. Then, instead, averaging of later variables is used, which are linear with respect to the model output, or alternatively, the process is maintained at high resolution instead.

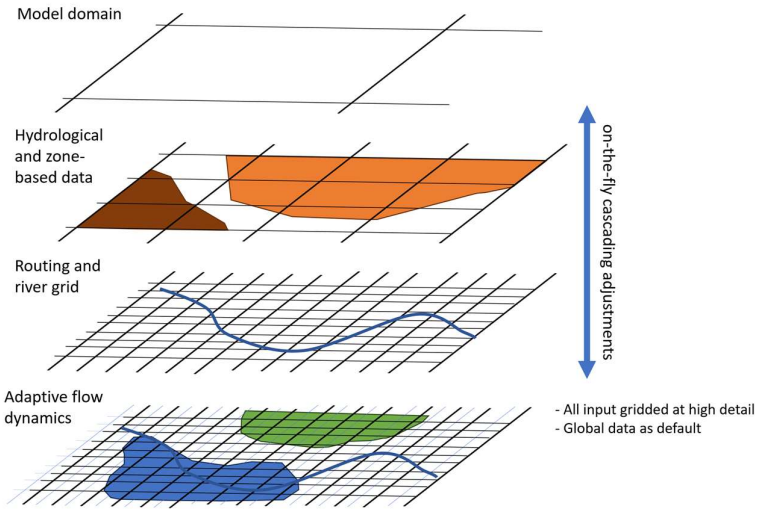

Figure 3 Grid adjustments for various processes as used by FastFlood

The final step of the FastFlood model is an artificial adaptation of the Saint-Venant. This step is carried out after the initial floodplain water distribution by means of the logarithmically cascaded profile approximations. This solver, for which details can be found in earlier work, has been adapted to function on an adaptive cascading grid.

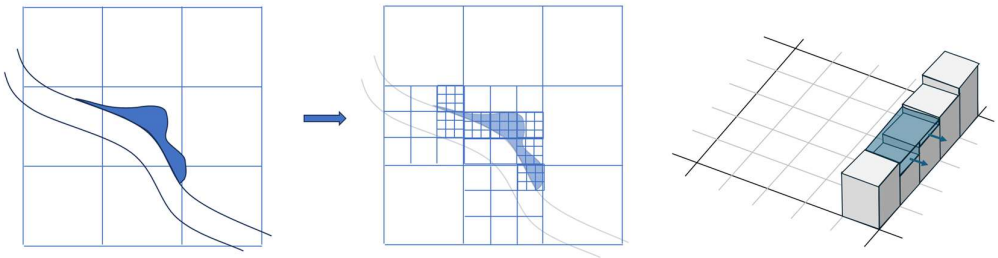

Figure 4 Adaptive noctree grid refinement scheme (left) and the need for estimation of partial flow through boundaries at the edge of a group of grid cells (right)

The final artificial Saint-Venant solution is carried out on an adaptive grid, before finally being refined for the full domain to full resolution as to provide full output file resolution and consistent file formatting.

[1] The elevation data is re-interpolated for river routing using a particular geometric consideration. Two effects can be important here, as the flow routing needs to follow channels with lower elevation values, but using minimum interpolation might remove obstacles from the data, while maximum interpolation might remove the actual flow paths. We take out of each 3x3 gridcell group that 3rd value, which is based on a geometric consideration. Any consistent high elevation feature that blocks water flow, must either have 2 pixels within the 3x3 cell group, and requires to be blocked, or alternatively, the feature will instead have 2 pixels with higher elevation in the neighboring 3x3 cell groups, and the water or routing will instead be blocked there.

Landscape parameters

Elevation and DTM Filtering

Our elevation dataset is a reprocessed version of Copernicus30, with a custom DTM filter that removes buildings and vegetation

We implement a new DTM filter particularly meant to remove buildings and vegetation from the elevation models, as these can effectively prevent water flow through urban and forested areas, and cause erroneous artefacts to develop in the final flood maps. These kind of data filters are known as DTM filters, which have been applied widely in various forms, in particular for the application of flow modelling (Hawker et al., 2022, Pronk et al., 2024). The approach shown here provides a novel implementation based on the sweeping algorithmic structure as deployed by FastFlood for hydrological correction of terrain. The sweeping algorithms, with simple but well-chosen update roles, can often provide useful processing steps with minimal compute requirements.

Here, two sweeping algorithms are developed, first, an isolated obstacle sweep filter. Here, sweeps move into the grid and update according to the rule (applied separately for each cardinal direction in the grid):

$$z_{i+1} = \max(z_{i-1} + \min(0, z_i - z_{i-1}), z_{i+1} + \min(0, z - z_{i+1}))$$

Secondly, a slope limiting sweep filter is implemented, with an update rule define as

$$z_{i+1} = \min\left(z_i + \min\left(S_{max}, (1.0 - w_{i+1})(z_{i+1} - z_i)\right), z_{i+1}\right)$$

Both filtering algorithms are combined with a weighted value based on a more typical slope-based object detection. Considering the abrupt changes in elevation caused by vegetation or buildings due to, often vertical, gradients along their edges, the variance of the slopes relative to the regional slopes are used to create a weighting factor for the filters.

$$w = \min\left(1.0, c_1 \frac{WindowVariance\left(DEM - WindowAverage(DEM, s_1)\right)}{WindowAverage(Slope(DEM), s_1)}\right)$$

Final height adjustments, during the algorithms, are limited to estimates of maximum viable building and vegetation height from the Global Building Height dataset (JRC) and the global canopy height raster data (NASA) to provide some guidance in terrain where isolated features are part of the landscape, but no buildings or vegetation is present.

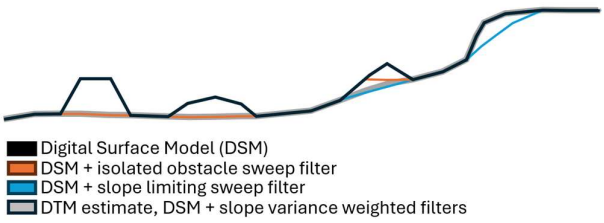

Figure 5 DTM filter as deployed through FastFlood

Example output of the filter is provided in appendix B.

Landscape parameterization

LandCover

Land cover information is provided through classified Sentinel-2 data, in particular the Copernicus WorldCover 10m dataset. Each class is linked with Manning's surface roughness value based on literature values. The presence of vegetation, supplemented with global forest cover and canopy height data, are in addition used to estimate leaf area index for interception estimations during the hydrological component of the model.

Precipitation

We use ERA5- Land, the fifth-generation global reanalysis from ECMWF, offering hourly global estimates of

atmospheric and land-surface variables on ~10 km grid from 1940 to near real-time (Muñoz-Sabater et al., 2021; ECMWF, 2017). GPM IMERG provides blended multi-satellite precipitation retrievals at 0.1° (~10 km) resolution every 30 minutes, including early, late and final runs calibrated against ground observations (Huffman et al., 2019; Zhou et al., 2023). This is used as the basis for the analysis of the spatial component of the rainfall statistics. ERA5 furthermore delivers surface temperature, humidity, soil moisture and radiation forcing.

Climate

The climate scenarios are based on a General-Extreme-Value analysis of the CMIP6 NASA downscaled climate model ensemble(thrasher et al., n.d.). A total of 20 models were used to carry out segmented-window GEV analysis, obtaining ratios between extreme precipitation of each return period for each time period (current, 2030, 2045, 2060, 2075, 2090, 2100). Based on these ratios, current period design events are adjusted using the bicubically interpolated relative changes most closely related to the actual return period and duration of the design event.

Soil and infiltration

We integrate SoilGrids v2.0, a global machine-learning soil mapping system at 250 m resolution, predicting properties like texture, organic carbon, density, pH and depth to bedrock, based on >230 000 soil profiles and environmental covariates (Hengl et al., 2017; ISRIC, 2017). Based on these soil characteristics, pedotransfer (saxton et al., 2006) functions are utilized to predict soil physical parameters. SMAP provides spaceborne L-band microwave retrievals of near-surface soil moisture. Together, these inform soil infiltration parameters and initial moisture state in subsurface and hydrological modeling.

Rivers and hydraulic structures

River discharge and hydraulic routing are informed using GLOFAS, the global flood forecasting system run by Copernicus Emergency Management Service and ECMWF, providing ensemble streamflow forecasts at ~0.05° resolution and flood hazard maps (Alfieri et al., 2013; ECMWF/Copernicus, 2022). GRDC datasets supply in-situ river discharge observations utilized for bias-corrected of the GLOFAS re-analysis datasets. Global Surface Water Explorer (GSWE) and Global Flood Database layers supply historical flood extents. These are used to calibrate and validate hydraulic and flood-routing components of the model.

Global riverine shapes are derived from combined Hydrobasins and Global River Mask From Landsat data. The OpenStreetMaps database is sampled for the location of culverts, and automatically placed in the local drainage grid.

Stormwater drainage capacity

For many areas around the world, protection against flood impact is in place. This can take many forms, but commonly feature either levee systems or urban stormwater drainage systems. Both are estimated here using the FLOPROS global protection level database, as well as the urban regions derived from OSM data as well as WorldCover 10m built-up classification. A stormwater drainage system is added to the setup for urban regions, with a capacity that equals the design event of the protection level specified in FLOPROS. In a similar approach, the width and depth of rivers are adjusted to implement the influence of levee systems in regions with a high protection level. The empirical power laws linking drainage area to river depth for each region of the globe are rescaled according to the protection level, with an empirical scaling derived from a subset of river depth samples under various protection levels.

Buildings

Building and roads are used to influence infiltration processes, as well as flow, through surface roughness, and provide exposure output. Both elements are obtained through the OpenStreetMaps dataset, in vectorized format. For modelling input, these are first rasterized before infiltration capacity of the regular soil is reduced to zero, and only stormwater drainage capacity is left for urban areas.

Overview

Domain	Dataset(s)	EO Sources / Usage	Satellite platforms
meteorological	ERA5, GPM IMERG	ERA5 for atmospheric/land surface forcing; IMERG for precipitation inputs	GPM sensors, satellites via ERA5 assimilation
Sub-surface and soil	SoilGrids, SMAP	SoilGrids for soil physical properties; SMAP for soil moisture state	SMAP soil moisture; SoilGrids based on in situ
Rivers & hydraulic structures	GLOFAS, GRDC, GSWE, Global Flood DB	GLOFAS for ensemble streamflow forecasts; GRDC for calibration; GSWE/flood DB for historical inundation, OpenStreetMaps data for culverts and local drainage routes	ERA5-forced GLOFAS; satellite imagery underlying GSWE
Surface and cover	Copernicus DEM (GLO-30, EEA-10), national DEMs , World cover	DEM data for elevation/surface slope; flood layers and Worldcover used to derive surface roughness	TanDEM-X derived Copernicus DEM; World cover based on Sentinel-1 and 2
Buildings and roads	Sentinel-2 imagery plus canopy/building height,	Sentinel–2 for mapping impervious urban infrastructure; ancillary EO for 3D modeling and hydraulic routing	Sentinel-2 (and optionally Sentinel-1 SAR fused)
Urban stormwater capacity & protection	FLOPROS	FLOPROS, river width, reservoir capacity, lake altimetry and IMERG precipitation feed urban drainage models	FLOPROS global database

Table 1 Overview of utilized datasets to carry out parameterization of the FastFlood model

Event scenarios

Multi-scale design storms for precipitation and snowmelt

Design events, when selected by the user, are derived from global re-analysis data (ERA5- Land). To address the generalized application of design events, either for precipitation or snowmelt, we introduced the usage of IDFS curves (Nubakulu et al., 2026) as a major extension of the idea of Area Reduction Factors (ARF) (Svensson & Jones, 2010; Wright et al., 2014). These are analogous to traditional IDF curves, but instead feature a variation of spatial sizes used for the analysis. Additionally, this multi-dimensional analysis approach aids in preventing some of the pitfalls in generalizing the multitude of potential storm events within the historical records (Wright et al., 2014). The analysis for the spatial component was carried out on GPM IMERG, a 20-year 3-hourly record. Based on this, a series of unique IDF curves was fitted for windows of 1 gridcell, 3 gridcells, 9 gridcells, 27 gridcells and 81 gridcells, with a gridcell size of ~11 km for GPM data. Finally, based on the required size for the design event, bicubic interpolation is carried out in the spatial dimension to obtain the IDF curves for the exact size, and then continue to generate Hyetographs as would usually be done using IDF curves. A highly usefull property of these spatial scaling components is that they furthermore reflect how the averaging taking place for large-region design events reduces the intensity compared to the actual localized extreme precipitation that is part of the event. Real events for larger basins, while having significantly lower extreme precipitation on average, have localized extremes significantly higher, which limits the fraction of infiltration taking place. The spatial scaling resulting from the IDFS curves characterize the relative difference between the large-scale lower average extremes and localized values that would be part of the same event. We utilize these relative changes to provide a virtual precipitation value to the infiltration calculations. This means we in fact deal with infiltration as if the event had the locally expected precipitation, while the large-scale routing and accumulation to the river system, as well as the final fluvial floods, still get the correct total design precipitation for the basin.

Baseflow, soil moisture

Soil moisture is initialized using historical data, utilizing NASA SMAP layers to ensure global coverage. For design events, monthly statistics derived from SMAP are employed. These events are situated within the median

soil moisture value of the wettest month to reflect the high frequency of flash flood occurrences during annual wet periods. The maximum moisture value is excluded to avoid overestimation; as peak moisture levels typically manifest post-flood, utilizing these values as initial conditions would result in a compounding of extreme precipitation effects.

Baseflow is derived from GLOFAS re-analysis data, calculated as the moving-window average of discharge values for the week preceding the event's onset (Feizi et al., 2022). In hazard map scenarios (design events), discharge is incorporated directly into the boundary conditions for river flow rates. This discharge is assumed to accumulate linearly per unit of drainage area upstream of the largest outlet within the model domain, thereby allowing the model to be warm-started with pre-existing discharge in the river system. For extended simulations, soil moisture content in riverine grid cells is linearly reduced by the baseflow.

Boundary conditions and placement

Placement and routing adjustment for large rivers

Discharge boundary condition placement is carried out starting with the incoming routes as taken from HydroBasins river lines (Lehner & Grill, 2013). These river lines, while available globally, feature a deviation from actual river center lines up to several Kilometres, and do not feature splitting rivers. We perform a series of search and match algorithms within nearby elevation data to find optimal placement pixels with lower elevation, indicating the riverbed is found. Discharge values are linked to GLOFAS pixels using a similar search and match based on drainage area, with a final correction applied for minor mismatches in terms of drainage area. The GLOFAS design values, as well as forecasts, are corrected with a bias correction using scaling factors based on return period values (a full extreme-value focused histogram transform).

A routing adjustment is carried out based on detected river splitting within the network. This is only required for the FastFlood static model, as the dynamic model will split river flow naturally based on the Saint-Venant equations. For the static model, river sections that deviate from main river lines are detected, and flow is split based on the proportional river branch widths.

Final data pipelines and parameterization

There are finally several primary options for using the FastFlood global system;

- Past
    - Hindcast
        - Using the data from the past to provide flood maps and information for any historic date since 01-01-2000.
- Present
    - Design event
        - Use design events, combining statistically representative input for precipitation, snowmelt and storm/tidal surge under current climate conditions
    - Forecast
        - Using the data from the past days to provide flood maps and information for the current day
- Future
    - Design event
        - Use design events, combining statistically representative input for precipitation, snowmelt and storm/tidal surge under climate change scenarios
    - Forecast
        - Use the latest snowmelt, precipitation and discharge forecast to predict flood maps and information for the coming two weeks relative to the current day.

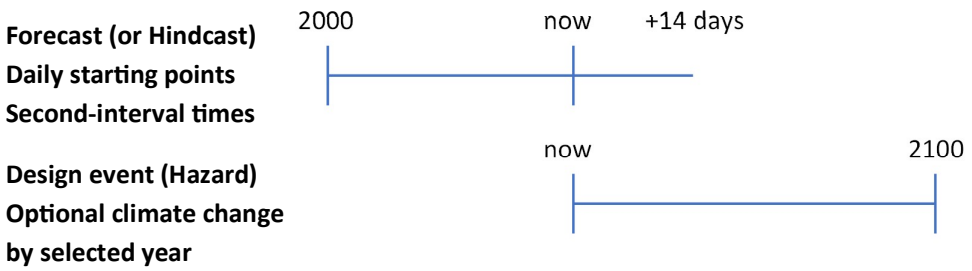

Figure 6 Schematic view of the time periods for which Fastflood Global can be used.

Finally, each of these is interactive, meaning that when the user provides some alterations, including

- Elevation changes: Barriers or reservoirs constructed directly by means of an altered elevation model. Can be provided as a vector dataset manipulated directly by the user.
- Flood protection: Alterations to channel dimensions and channel properties that can reflect potential flood protection
- Drainage system: Alterations to the existence or capacity of stormwater drainage systems, or river and channel routes.
- Nature-based solutions: Alterations to soil and vegetation information layers provided, with default values based on recent literature for many common types of NBS.

Results and analysis

The following section showcases some of the applications of the model to extreme events around the world. The section outlines the model capabilities by providing an example use case how it can be used for different time periods like past present and future

Past: Local flood time-series

Geul floods 2021

In June 2021, many parts of western Europe experienced severe flooding due to intense precipitation; one of the regions affected in the event was the city of Valkenburg in the Netherlands (Mohr et al., 2023). We used the FastFlood Global with its out-of-the-box parametrization to model the resulting flood for the event. Figure 7 indicates the system's output, including the peak velocities and depths. The outputs show a good fit with the dron-based flood extent for the event, reaching a percentage accuracy of 94%.

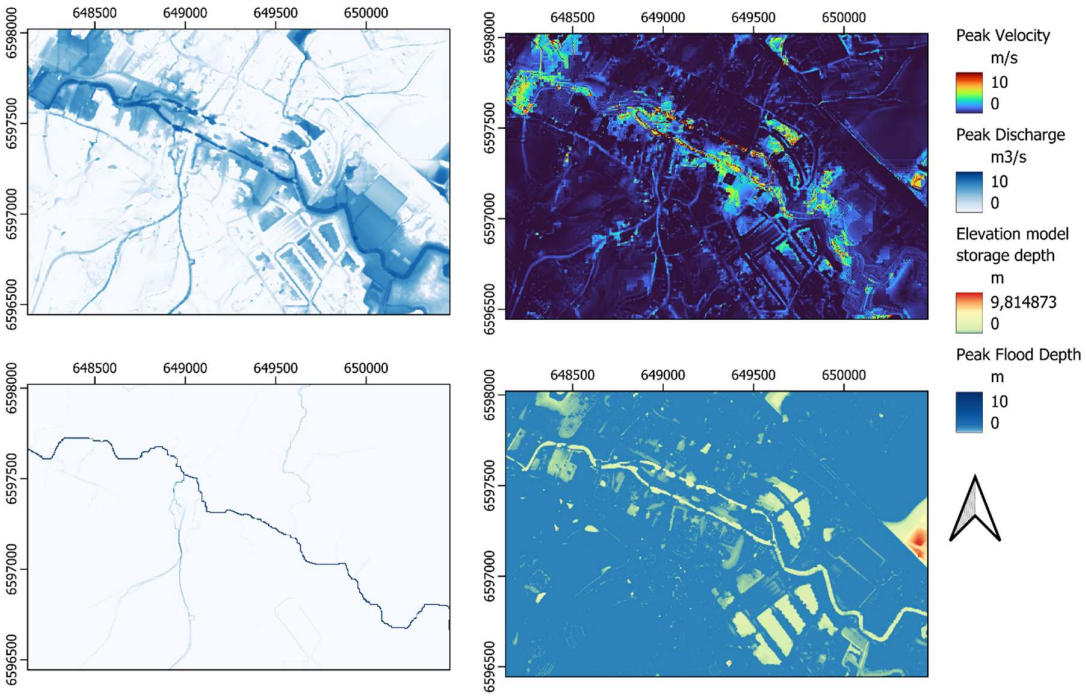

341

342 *Figure 7 Flood modelling output for the city of Valkenburg, peak flood depth (Top left), peak velocity (Top right),*
343 *peak discharge (Bottom left), and elevation depression storage (Bottom right). Note that these depressions are*
344 *corrected for by the pre-processing algorithms (e.g. hydrocut/hydrofill/routing)*

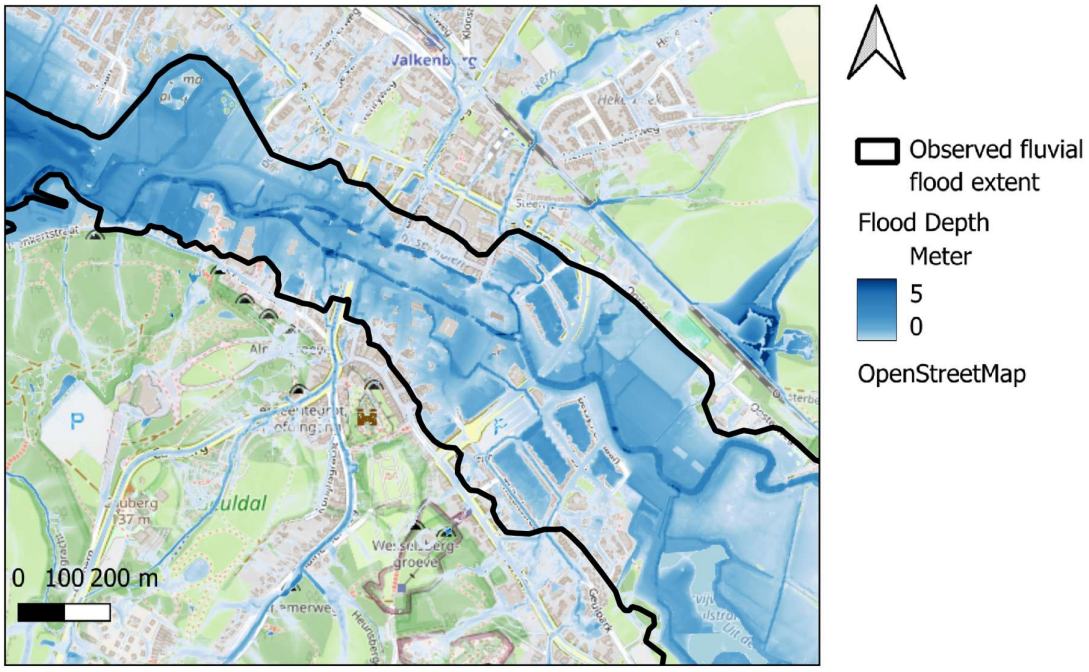

345

346 *Figure 8 Comparison of the uncalibrated flood model output with the observed flood extent (observations where only*
347 *mapped for the main Geul river in this region).*

The web-based tooling around the model allows the usage of the modelling system for interactive exploration of alternative scenarios, visualized in Figure 14 for this region, with a 3D perspective view of the zero-configuration available flood map output.

Figure 9 The FastFlood global interactive features allowing users to add adaptations within the landscape and explore in rapid fashion the consequences of these changes.

Present: Hazard mapping

Cambodia flood hazard

Another application of the model is presented here, for the country of Cambodia, utilizing the system for a national flood hazard mapping effort. Figure 11 shows the input parameters including elevation data, surface roughness and the infiltration rate. a hazard mapping example using the FastFlood global system at an alternative scale. Predominantly, the out-of-the-box system is utilized here, with some key exceptions. Here, special attention was given to the dynamics between the Mekong river and the Tonle Sap lake, where reverse flow significantly increases flood extents around the lake. Here, the peak lake levels are based on satellite-derived water surface altimetry, that captures the lake storage despite the pseudo-static nature of the FastFlood model.

Figure 8 shows the global river network, based on a combination of Hydro Basins and Global River Centerlines from LandSat.

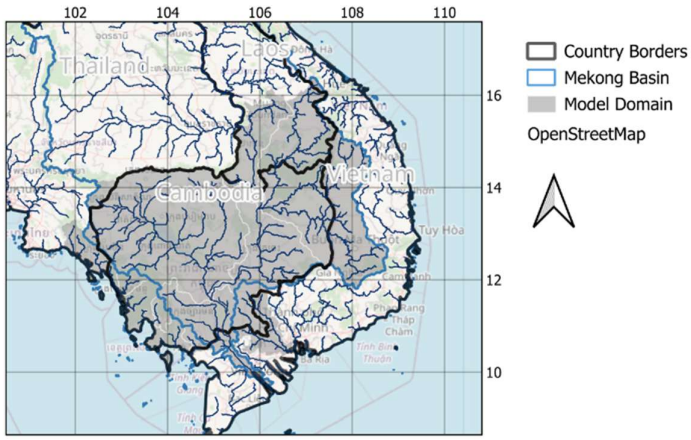

Figure 10 The global river datasets, merging hydro basins and river centrelines from Landsat data, as used for the automated setup for Cambodia.

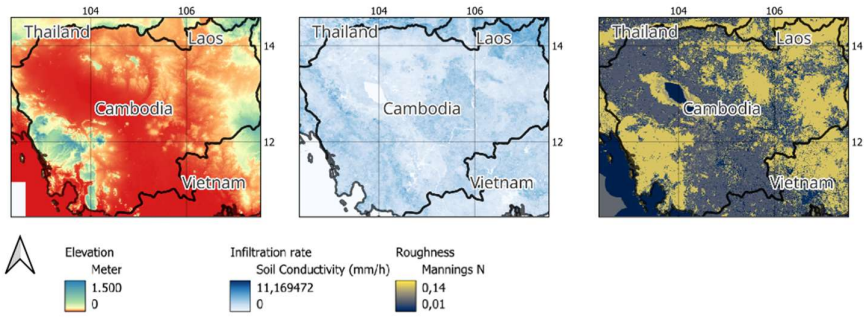

Figure 11 Input parameters, landscape layers, for the Cambodia flood modelling; elevation data, infiltration rates for the second soil layer, and surface roughness.

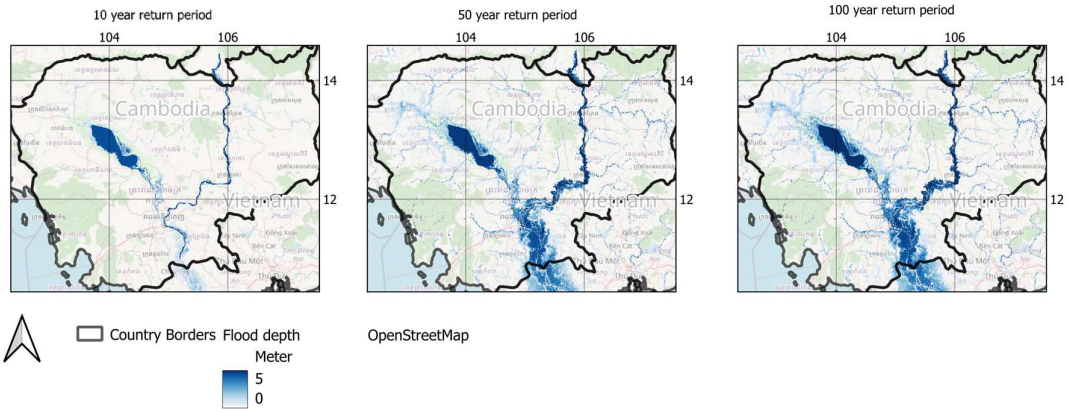

Figure 12 Cambodia national-scale flood hazard maps at 20 meter resolution, visualized for 20, 50 and 100 year return periods.

Climate change was addressed for the region, with additional flood simulations carried out with adjusted precipitation input. Figure 12 indicates the climate change trends on relative increases of extreme precipitation for various scenarios and durations of precipitation.

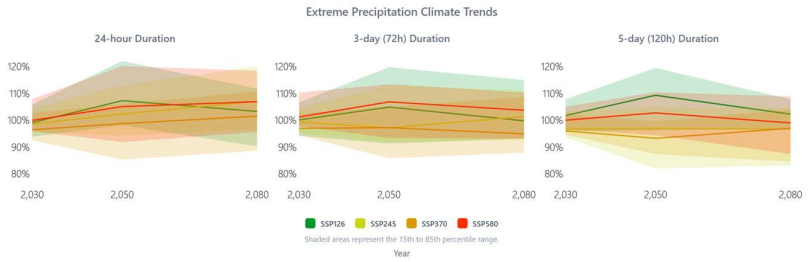

Figure 13 Climate change scenarios, and their influence on extreme precipitation intensity in the region of Pnom Phen, with quantile 15 and 85 ranges within the CMIP6 NASA NEX-GDDP downscaled ensemble.

Future: Forecasting

The model was applied for forecasting in the case of the 2024 Kazakhstan spring snowmelt floods. Figure 13 shows the application of the automated parameterization of the FastFlood global system to the region around Atbasar, along the Ishim river. Discharge boundary conditions here are based on bias-corrected glofas forecasts, with automated placement and setup of appropriate mass and momentum flow boundary conditions for the advection calculations within the model. The model is applied here in an uncalibrated manner, and compared directly with sentinel-2 based flood extents, taken at the available date that most closely matches the peak of the flood extent in this region. The resulting modelled flood extents give a 99.4% accuracy compared to observations.

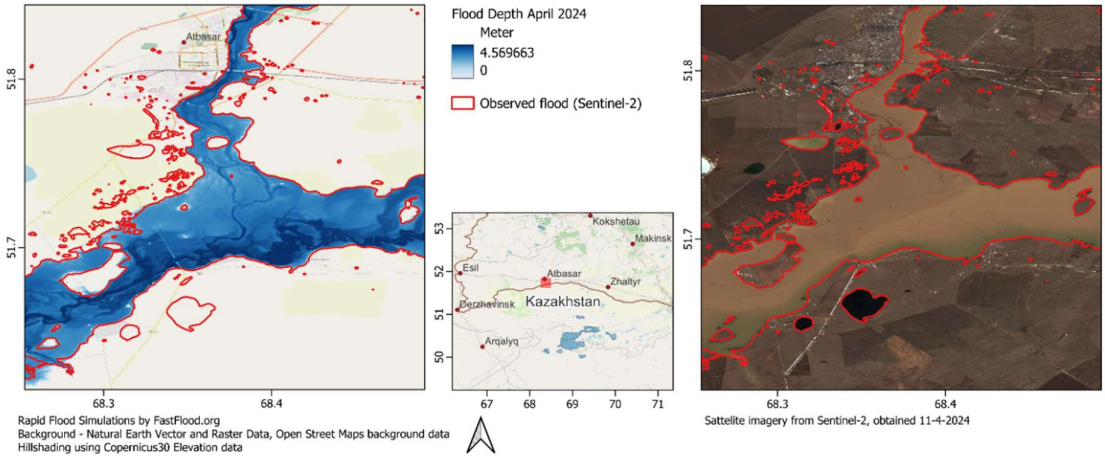

Figure 14 Flood forecast results for the Ishim river, and the spring 2024 snowmelt driven floods in Kazakhstan around Atbasar.

Emergency Mapping

Due to the calculation speed of the model, rapid application is possible in the context of emergency mapping. The provided figures illustrate the FastFlood Global system's critical utility in emergency response scenarios, specifically its capacity to generate immediate, accurate flood intelligence in data-scarce environments.

Bangladesh 2024: Bridging Observational Gaps

The first figure (Figure 15) presents a comparative analysis between post-event Sentinel-1 Synthetic Aperture Radar (SAR) imagery and FastFlood simulations for the June 2024 Bangladesh floods.

- **Observational Constraints:** While satellite-based tools like Sentinel-1 provide essential ground truth, they are limited by satellite revisit times and data processing latency.

- **Predictive Value:** The FastFlood simulation (Right) demonstrates a high degree of spatial agreement with the radar intensity observations (Left), accurately capturing complex inundation patterns across the delta. In an emergency context, this allows responders to generate reliable inundation maps minutes to hours before satellite imagery becomes available, filling critical information gaps during the initial response phase.

Rapid Assessment and Calibration

The second figure (Figure 16) highlights the system's speed during the immediate aftermath of a disaster, visualizing a rapid simulation calibrated against high-resolution PlanetLabs optical imagery (12-09-2023).

- **Speed of Deployment:** This application demonstrates the ability to calibrate the model against space-derived observations within a timespan of just a couple of minutes.

- **Operational Utility:** By rapidly assimilating available visual data to tune the model, the system provides immediate estimates of flood depth and extent in complex urban environments. This capability is vital for directing rescue operations to the most severely impacted zones when local ground data is disrupted or non-existent.

Together, these applications provide initial validation of the system's role in Emergency Mapping, where calculation speed facilitates rapid situational awareness that static maps or slower traditional models cannot provide.

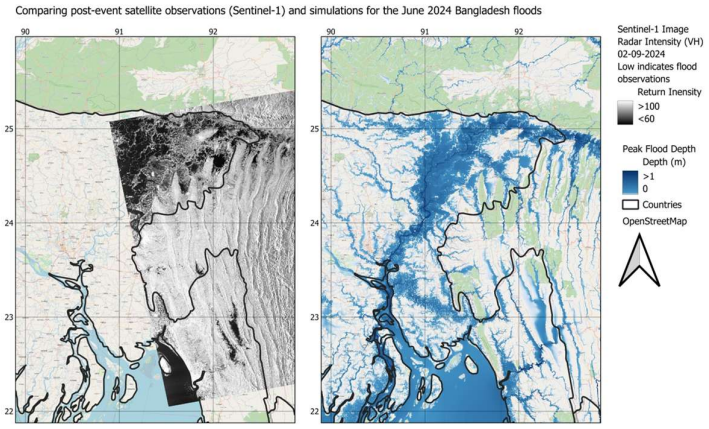

Figure 15 Flood modelling results, utilising the FastFlood Global system, for the Bangladesh floods in summer 2024 (Right), and Sentinel-1 VH intensity, where darker areas indicate water presence (Left).

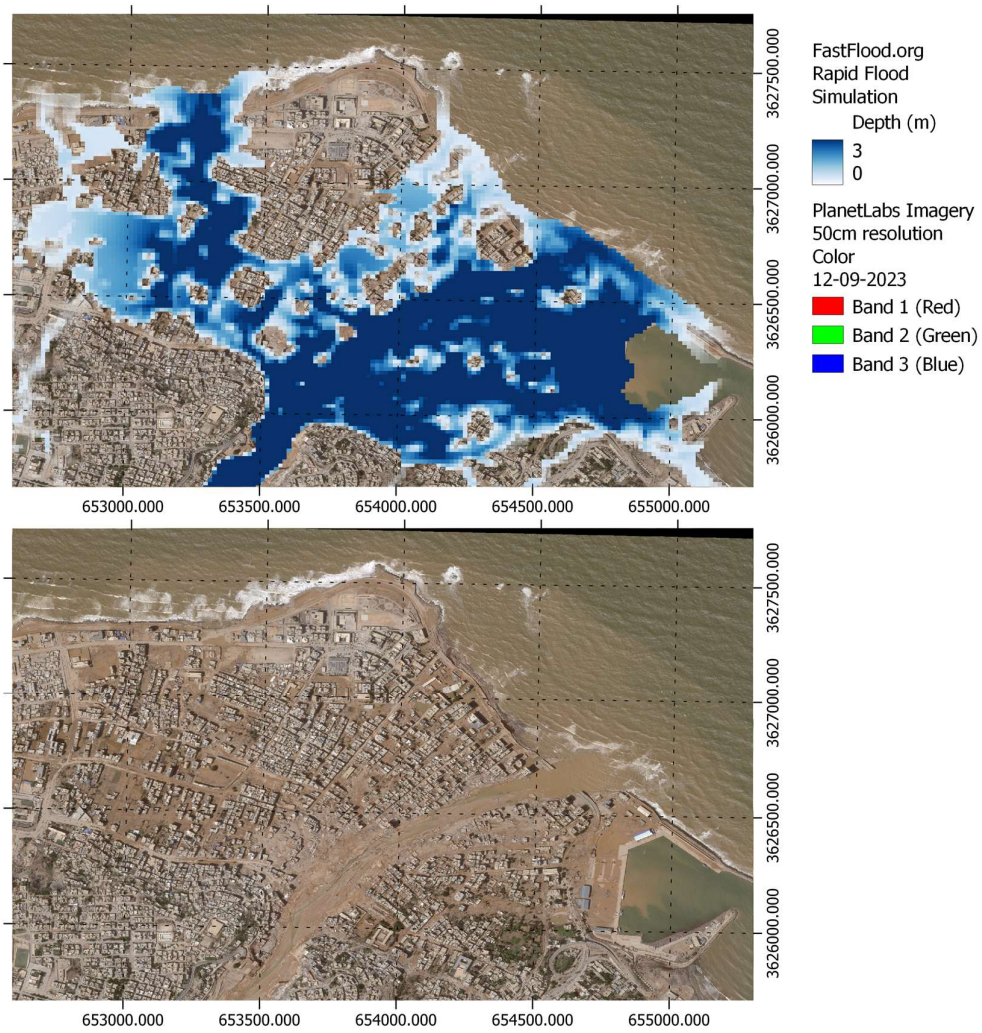

Figure 16 Rapid flood modelling assessment, calibrating the FastFlood output within a time-span of a couple minutes on space-derived observations.

Discussion

Comparative Review of FastFlood Global and Existing Flood Information Systems

The FastFlood Global system integrates rapid hydrodynamic modelling with automated global parameterization, distinct from existing static or operational frameworks. A comparative analysis against established categories follows:

- **Global Hazard Information Layers (Fathom, JBA, FirstStreet):** These platforms provide high-resolution, static hazard maps essential for risk baselines and trend analysis. However, they rely on pre-computed scenarios, prohibiting real-time adjustment. In contrast, FastFlood Global utilizes a dynamic core to allow interactive simulation of user-defined changes—such as new infrastructure or nature-based solutions—facilitating immediate feedback on adaptation scenarios rather than static viewing.

- **Global Flood Forecasting Systems (JRC GloFAS, Google Flood Hub):** Operational systems like GloFAS operate at coarse resolutions (~5 km) suitable for basin-scale discharge but limiting for local impact assessment. Google Flood Hub improves locality but typically relies on AI or pre-calculated libraries. FastFlood bridges this gap by downscaling coarse forecast data (e.g., GloFAS discharge) into

high-resolution (10 m) hydrodynamic inundation maps, maintaining physical consistency through automated boundary condition coupling.

- **Real-time Response Tooling (Sentinel-based, ICEYE):** Satellite-based observation offers critical situational awareness but is constrained by revisit times and cloud cover latency. FastFlood complements these tools by providing predictive modelling to fill observational gaps. Validation against Sentinel imagery for recent events (e.g., Kazakhstan 2024) demonstrates high spatial agreement (99.4%), indicating its utility as a rapid proxy when direct observation is unavailable.

- **Adaptation Tools and Models (HEC-suite, MIKE, LISEM):** Traditional solvers provide high-fidelity physics for engineering but require extensive manual setup and computational resources. FastFlood reduces setup barriers via automated global parameterization (synthesizing ERA5, SoilGrids, etc.). Benchmarking against the LISEM solver confirms comparable accuracy (~98% flood extent overlap) with a computational speed increase of approximately three orders of magnitude (e.g., reducing runtime from ~8 hours to 25 seconds for Dominica), enabling ensemble-based uncertainty analysis.

Model Consistency and Uniformity

The interactive nature of the FastFlood Global system precludes the use of static, pre-calculated data layers. Consequently, maintaining consistency across variable spatial and temporal scales requires a targeted approach.

Spatial Consistency The spatial consistency of simulated flood intensities is of particular concern when altering model domains (extent) or resolution. While the physically-based formulation of the FastFlood Global system is designed to minimize resolution dependence, sensitivity to grid size is an inherent characteristic of numerical flood models. Lower-resolution simulations inevitably degrade the representation of critical terrain features. However, these effects are mitigated within the model through an automatic transition to a coupled 1D-2D system, which ensures adequate throughflow even in complex terrain represented at coarser resolutions.

Temporal Consistency Temporal inconsistencies may arise from the divergence between the datasets used for design events and real-time forecasting. Design events rely on Intensity-Duration-Frequency (IDF) curves derived from 80 years of ERA5-LAND reanalysis data, whereas forecasts are generated using the ECMWF ensemble. although extreme precipitation statistics between these datasets are comparable, they are not identical. It has been noted that ERA5 reanalysis data can underestimate precipitation extremes, particularly for small-scale, high-return-period events. Future improvements to the model accuracy could be achieved through bias correction of the IDF curves using global hourly precipitation station datasets.

Boundary Condition Consistency A specific challenge involves the parameterized consistency between a full-basin hydrological simulation and a truncated domain (e.g., a river section) relying on external boundary conditions. A full-basin domain generates discharge endogenously via the FastFlood hydrological computation. Conversely, a truncated domain utilizes bias-corrected GLOFAS design discharge events. While conceptually similar in terms of water balance, results from the internal hydrology are not guaranteed to match the bias-corrected GLOFAS inputs used for river sections. The use of bias-corrected data allows the model to remain linked to observational records, thereby maximizing accuracy. To address potential inconsistencies, the current approach involves the automatic calibration of the inner model against global re-analysis design events. An alternative method—developing fully consistent hydrology and routing between the inner model and the global re-analysis model—remains a critical area for future development of the modelling system.

Quality and Uncertainty

The computational efficiency of the modelling approach facilitates the execution of ensemble simulations. This capability is critical for capturing the range of potential flood scenarios resulting from uncertain meteorological triggers. While limitations persist due to the global scope of the system—specifically regarding the incorporation of local water management infrastructure—the presented work represents a significant advancement in the coverage and feature set of global flood modelling. Furthermore, the integration of ensemble forecasts and probabilistic hazard simulations enhances the quantification of model uncertainty.

Global Forecasting and Early Warning Implications

The implementation of this flood modelling system within a web-based platform provides access to detailed global flood forecasts. By leveraging existing datasets and technologies, the system aims to maximize accuracy and reliability while maintaining global coverage. However, the accessibility of such data raises ethical questions regarding mandates, governance, and liability.

It is emphasized that the presented work is strictly distinct from an operational Early Warning System (EWS). The platform is designed to provide detailed forecast information to users without issuing official warnings. The operational objective is to supplement available information for users with specific technical requirements, without interfering with the established protocols of water management agencies and mandated disaster response bodies.

While there is functional overlap between the FastFlood Global system and an EWS—such as the forecast-based calculation of expected flood intensity—fundamental differences remain. The technical modelling component constitutes only a subset of a complete EWS, which fundamentally relies on institutional capacity, effective dissemination channels, and community response mechanisms. With further validation across diverse sites and evaluation over extended periods, the proposed approach could potentially be adapted to support official early warning functions.

Conclusion

The presented FastFlood Global system provides a major step in the field of flood information technology, in particular due to its global coverage, interactivity, ability to reach very high resolution where data is available, and instant forecasting functionality. The model combines key parts of the rapid flood model FastFlood, with even faster application due to the usage of cascading grids, and a automated parameterization scheme based on numerous global and space-derived datasets. The quality of the models output

There are numerous limitations to the current methodology, which can be grouped in several categories

- Inconsistent output between past/future, design/forecast, due to the use of various datasets with inconsistent biases and characteristics
- Out-of-the-box performance and calibration limitations might limit accuracy depending on the area.

Perhaps most important of all considerations is this; To users untrained in the usage of flood models, these kind of systems can seem to offer a prediction that might be taken as “truth”, while containing limitations and inaccuracies due to the underlying assumptions and data limitations associated to this or any other model. The danger posed by inaccurate forecast without appropriate communication of limitations and uncertainties can erode trust in these types of modelling tools. While these objections similarly can be true for static traditional flood maps, the system presented here aims to provide close to expert-level interactive rapid tooling for a wide audience. In industry applications, the reality is that a variety of subsidies, regulations, assessments, risk reduction and management tasks require the use of flood models, often with highly limited resources, resulting in sub-standard quality results. The presented tools can provide a major step forward in bringing more advanced flood technology to new sectors, markets and communities.

Appendix A: Comparison of the improved FastFlood performance

To highlight the performance improvements, and the relative performance changes in terms of accuracy and calculation speed, the FastFlood model was applied to two flood events with and without the used of the cascading grid structure.
The first of these is the 2009 floods in the Fella basin, described in more detail by Bout & Jetten (2018) , together with a collection of reference simulation output utilizing traditional saint Venant solvers (as contained in the model LISEM) The total computational grid for this region consists of 1716 x 1526 pixels at 10 meters resolution. Simulation output is shown in Figure 15, with an observed FastFlood model runtime difference of 19.735 seconds vs 5.49 seconds.

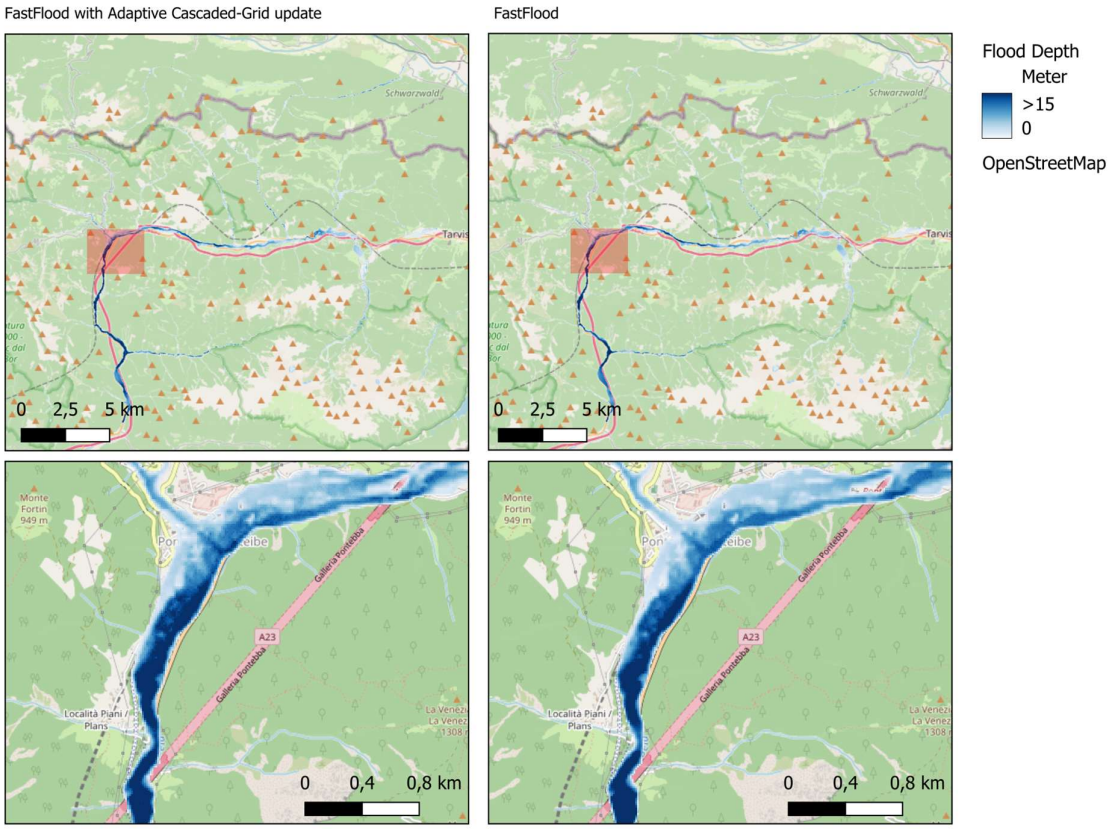

Figure 17 Comparison of the FastFlood model with and without the usage of the cascading grid approach, applied to the 2009 floods in Fella basin, Italy.

The pixel-wise percentage accuracy of flood extent between the usage of the cascaded grid refinement approach against a full traditional model is as follows

Table 2 Relative comparison of the updated fastflood model, as well as compute time for the Fella basin.

Fella	Flood Extent	Flood Depth	Compute time
Reference Saint Venant (LISEM)	100%	100%	29880
FastFlood	98.3%	98.1%	19.7
FastFlood GLobal	98.1%	97.3%	5.49

The second comparison case is the Caribbean island of Dominica. Here, the entire island with a 5 meter resolution DTM, and a grid resolution of 5211 x 9603 pixels was used. A final runtime difference was observed of 6444 seconds against 25 seconds.

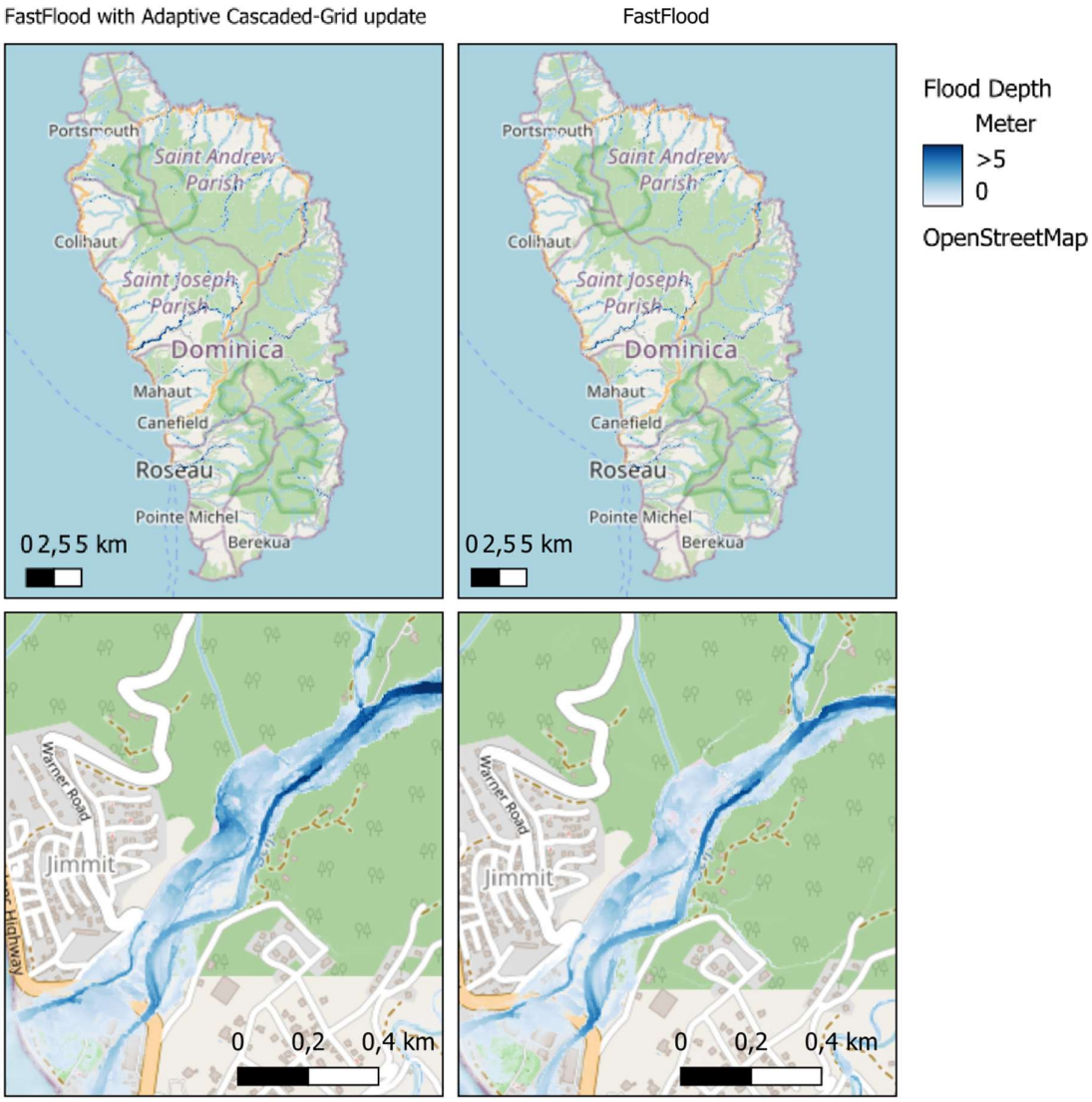

Figure 18 Comparison of the FastFlood model with and without cascading grid, as applied to a hurricane event on Dominica.

Table 3 Relative comparison of the updated fastflood model, as well as compute time for the country of Dominica.

Dominica	Flood Extent	Flood Depth	Compute time
Reference Saint Venant (LISEM)	100%	100%	122760
FastFlood	93.1%	98.1%	6444
FastFlood GLobal	98.1%	97.3%	25

Appendix B: DTM filter visualization

The elevation model filter results apply globally, and are visualized here for a region in the Netherlands and United States of America (Chicago). Both cases the algorithms are applied to the Copernicus30 DSM data, with input at approximately 30 meters resolution, and output at 20 meter resolution.

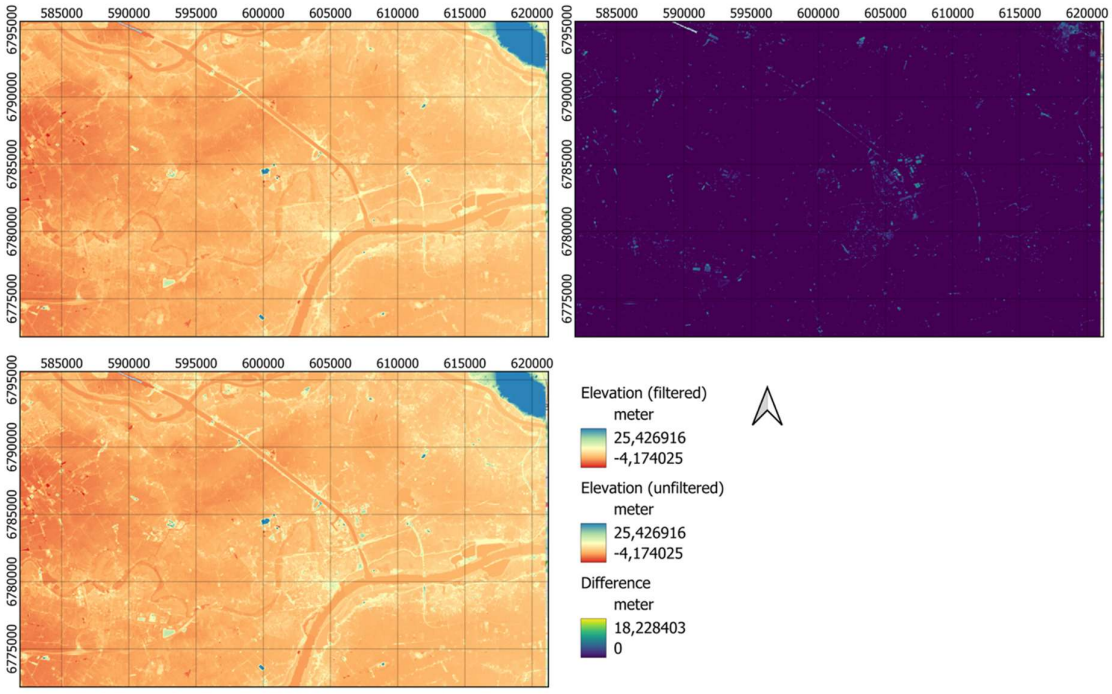

Figure 19 DTM filter application, and elevation model differences for DTM and DSM, applied to Copernicus 30 data in the Netherlands.

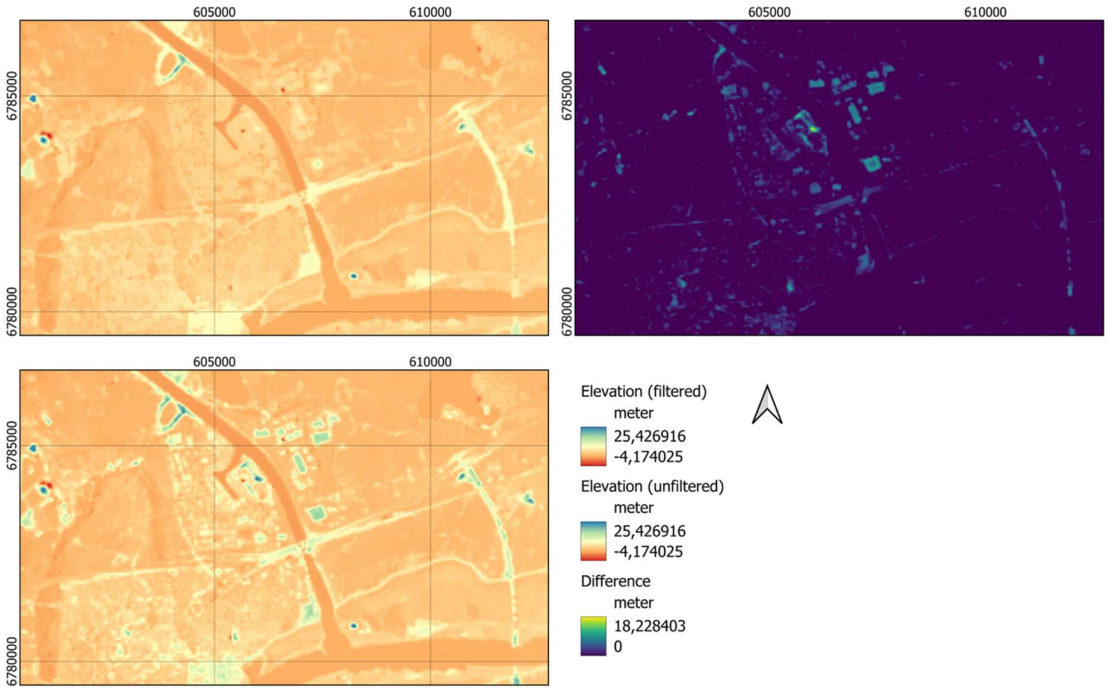

557

558 *Figure 20 DTM filter application, and elevation model differences for DTM and DSM, applied to Copernicus 30 data in the*
559 *Netherlands.*

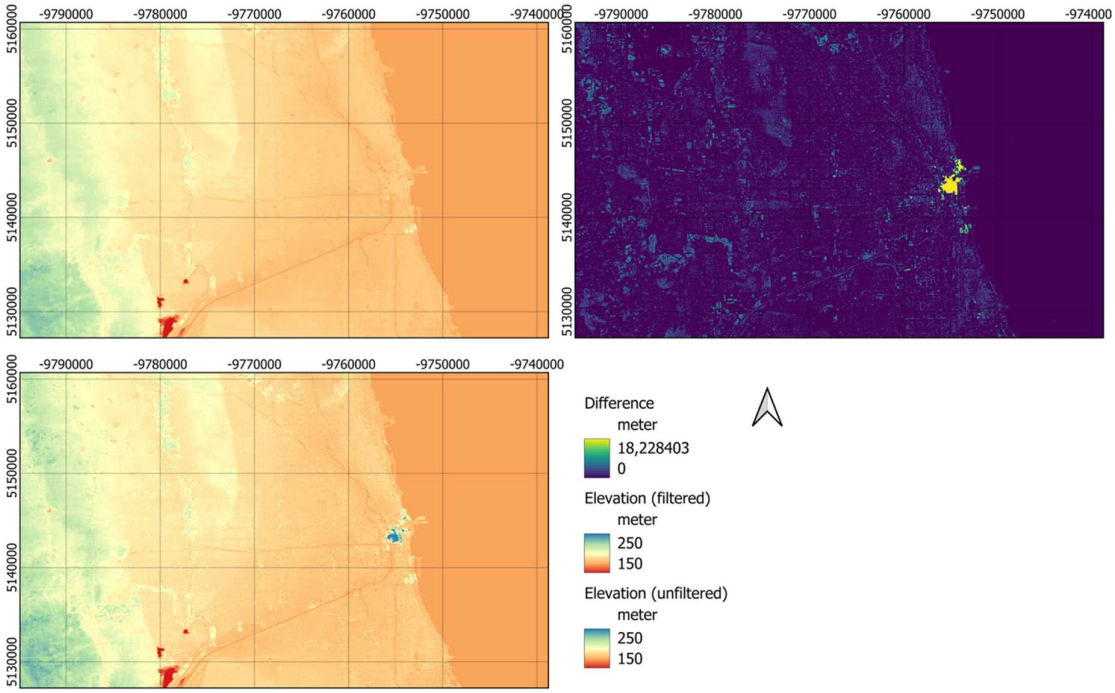

560

561 *Figure 21 DTM filter application, and elevation model differences for DTM and DSM, applied to Copernicus 30 data in the*
562 *USA (Chicago).*

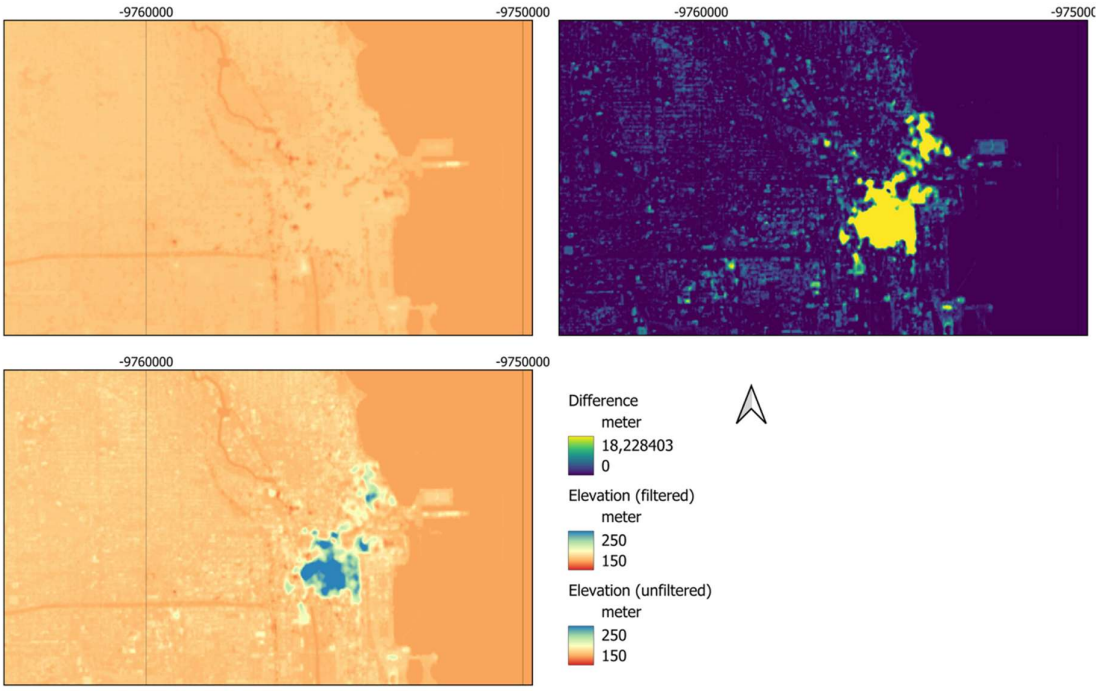

Figure 22 DTM filter application, and elevation model differences for DTM and DSM, applied to Copernicus 30 data in the USA (Chicago).

References

Alfieri, L., Burek, P., Dutra, E., Krzeminski, B., Muraro, D., Thielen, J., & Pappenberger, F. (2013). Global ensemble streamflow forecasting and flood early warning. *Hydrology and Earth System Sciences*, 17, 1161–1178.

ECMWF (2017). ERA5: data documentation. European Centre for Medium-Range Weather Forecasts.

ECMWF/Copernicus (2022). GloFAS user guide. Copernicus Emergency Management Service.

Hengl, T., et al. (2017). SoilGrids250m: Global gridded soil information based on machine learning. *PLOS ONE*, 12(2), e0169748.

Huffman, G., Kidd, C., et al. (2019). IMERG: Integrated Multi-Satellite Retrievals for GPM precipitation products. *Remote Sensing* Journal.

Muñoz-Sabater, J., et al. (2021). ERA5-Land: a state-of-the-art global reanalysis dataset for land water and energy cycles. *Earth System Science Data*, 13, 4349–4383.

Sentinel-2 technical studies (2019). Multi-temporal Sentinel-2 data for urban impervious surface mapping. *ISPRS Archives*.

Various case studies (2022). Case study using Sentinel-2 for urban land cover classification with interpretable machine learning. *RS&AS*.

ISRIC (2017). SoilGrids technical FAQ and mapping documentation. International Soil Reference and Information Centre.

Alfieri, L., Burek, P., Dutra, E., Krzeminski, B., Muraro, D., Thielen, J., & Pappenberger, F. (2013). Global ensemble streamflow forecasting and flood early warning. *Hydrology and Earth System Sciences*, 17, 1161–1178.

Cohen, D. et al. (2024). An improved flood forecasting AI model, trained and evaluated globally. Google Research Blog.

Google Research. (2024). Flood forecasting: AI for information & alerts. Google Flood Forecasting resource documentation.

Bates, P. D., Neal, J., Sampson, C., Smith, A., & Trigg, M. (2018). Progress toward hyperresolution models of global flood hazard. In Risk modeling for hazards and disasters (pp. 211-232). Elsevier.

Yamazaki, D., Watanabe, S., & Hirabayashi, Y. (2018). Global flood risk modeling and projections of climate change impacts. Global flood hazard: applications in modeling, mapping, and forecasting, 185-203.

Pekel, J. F., Cottam, A., Gorelick, N., & Belward, A. S. (2016). High-resolution mapping of global surface water and its long-term changes. Nature, 540(7633), 418-422.

Kettner, A. J., Brakenridge, G. R., Schumann, G. J., & Shen, X. (2021). DFO—flood observatory. In Earth observation for flood applications (pp. 147-164). Elsevier.

Harrigan, S., Zsoter, E., Alfieri, L., Prudhomme, C., Salamon, P., Wetterhall, F., ... & Pappenberger, F. (2020). GloFAS-ERA5 operational global river discharge reanalysis 1979–present. Earth System Science Data Discussions, 2020, 1-23.

Kuipers, E., Oldenburg, V., Sutanudjaja, E., Phung, P., Ficchì, A., & van den Homberg, M. (2025, March). Assessing the riverine flood forecast skill of GloFAS and Google Flood Hub with impact data and river flow observations to support early actions in Mali. In EGU General Assembly 2025.

Nearing, G., Cohen, D., Dube, V., Gauch, M., Gilon, O., Harrigan, S., ... & Matias, Y. (2024). Global prediction of extreme floods in ungauged watersheds. Nature, 627(8004), 559-563.

Ho, Y. F., Grohmann, C. H., Lindsay, J., Reuter, H. I., Parente, L., Witjes, M., & Hengl, T. (2025). Global Ensemble Digital Terrain modeling and parametrization at 30 m resolution (GEDTM30): a data fusion approach based on ICESat-2, GEDI and multisource data.

Poggio, L., De Sousa, L. M., Batjes, N. H., Heuvelink, G. B., Kempen, B., Ribeiro, E., & Rossiter, D. (2021). SoilGrids 2.0: producing soil information for the globe with quantified spatial uncertainty. Soil, 7(1), 217-240.

Feizi, H., Apaydin, H., Sattari, M. T., Colak, M. S., & Sibtain, M. (2022). Improving reservoir inflow prediction via rolling window and deep learning-based multi-model approach: case study from Ermenek Dam, Turkey. Stochastic Environmental Research and Risk Assessment, 36(10), 3149-3169.

Pronk, M., Hooijer, A., Eilander, D., Haag, A., de Jong, T., Vousdoukas, M., ... & Eleveld, M. (2024). DeltaDTM: A global coastal digital terrain model. *Scientific Data*, *11*(1), 273.

626 Hawker, L., Uhe, P., Paulo, L., Sosa, J., Savage, J., Sampson, C., & Neal, J. (2022). A 30 m global map of
627 elevation with forests and buildings removed. *Environmental Research Letters*, *17*(2), 024016.

628 Wright, D. B., Smith, J. A., & Baeck, M. L. (2014). Critical examination of area reduction factors. *Journal of*
629 *Hydrologic Engineering*, *19*(4), 769-776.

630 Svensson, C., & Jones, D. A. (2010). Review of methods for deriving areal reduction factors. *Journal of Flood*
631 *Risk Management*, *3*(3), 232-245.